24th COBEM - 2017

24th ABCM International Congress of Mechanical Engineering
December 3-8, 2017, Curitiba, PR, Brazil

COBEM-2017-1313
GÖRTLER INSTABILITY STUDY ON THE PRESSURE SURFACE OF A TURBINE BLADE

L. F. Marques
J. K. Rogenski
L. F. Souza
University of São Paulo, Av. Trabalhador São Carlense, 400, São Carlos, Brazil
laraposmac@gmail.com, josuelkr@gmail.com, lefraso@gmail.com

Abstract. *High-order, pseudo-spectral numerical code (Hope) is used to investigate the influence of the spanwise wavelength variations on the development of Görtler vortices considering a surface with curvature of variable radius. Due to non-linearities the effects caused by these vortices distort the boundary layer structure by modifying the streamwise velocity component in both spanwise and normal to the wall directions. The geometry considered in this study was adapted from the turbine blade geometry used in an experimental work present in the literature. Results show that the size of the vortical structures is an important parameter on transition process.*

Keywords: *Görtler vortices, spanwise wavelength, turbine blade, curvature variation, Direct Numerical Simulation*

1. INTRODUCTION

Flows over concave surfaces are present in several applications, and an important example are the turbine blades. Gas turbine blades are three-dimensional objects operating in a complex flow field. In the last decades both designers and researchers have been engaged in developing more efficient gas turbines.

It is known that on boundary layers over concave walls may occur laminar-turbulent transition phenomenon and this centrifugal instability mechanism may lead to the formation of a system of streamwise, counter-rotating vortex pairs known as Görtler vortices. Different approaches related to this subject have been presented both in theoretical studies as well as in computational studies. In this context, the goal of the present work is to carry out the analysis of Görtler instability up to a highly nonlinear region using a high-order numerical method to solve the Navier-Stokes equations. Through this analysis we intend to investigate the behavior of Görtler vortices with different spanwise wavelengths, $\lambda_1^* = 7.24 \times 10^{-4}\ m$, $\lambda_2^* = 10.631 \times 10^{-4}\ m$ and $\lambda_3^* = 16.414 \times 10^{-4}\ m$ when submitted to a variable curvature geometry represented by the pressure side of a turbine blade shown in Fig. 1.

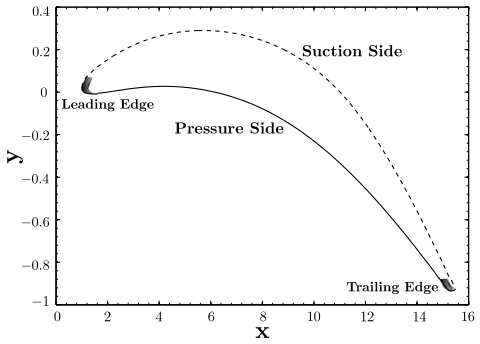

Figure 1. Turbine blade geometry adapted from Wang *et al.* (1997)

2. PROBLEM FORMULATION

A two-dimensional boundary layer flow over the pressure side of a turbine blade was consider. The problem is modeled through a Navier-Stokes system of equations written in vorticity-velocity formulation. For stability analysis, we assume

that vorticity and velocity components are the superposition of a baseflow and a disturbance represented by

$$\widetilde{g} = g_b + g,$$

where $\widetilde{g} = \{\widetilde{u}, \widetilde{v}, \widetilde{w}, \widetilde{\omega}_x, \widetilde{\omega}_y, \widetilde{\omega}_z\}$ corresponds to the total amounts of velocity and vorticity components, g_b denotes the baseflow and the disturbance is represented by g. In this formulation the linear and nonlinear terms can be isolated. This facilitates stability analysis of any baseflow.

Defining the vorticity as the negative curl of the velocity, and using the fact that both, the velocity and the vorticity fields are solenoidal, we obtain the following dimensionless vorticity transport equations in the streamwise (x), wall-normal (y) and spanwise (z) directions (Souza *et al.*, 2004) :

$$\frac{\partial \omega_x}{\partial t} + \frac{\partial a}{\partial y} - \frac{\partial b}{\partial z} + \frac{Go^2}{\sqrt{Re}}\frac{\partial d}{\partial z} = \frac{1}{Re}\nabla^2\omega_x, \tag{1}$$

$$\frac{\partial \omega_y}{\partial t} + \frac{\partial c}{\partial z} - \frac{\partial a}{\partial x} = \frac{1}{Re}\nabla^2\omega_y, \tag{2}$$

$$\frac{\partial \omega_z}{\partial t} + \frac{\partial b}{\partial x} - \frac{\partial c}{\partial y} - \frac{\partial}{\partial x}\frac{Go^2 d}{\sqrt{Re}} = \frac{1}{Re}\nabla^2\omega_z. \tag{3}$$

We consider as relevant nondimensional parameters the Re, Go, and Λ, known as Reynolds and Görtler numbers, and spanwise vortex wavelength defined respectively by

$$Re = \frac{U_\infty^* L^*}{\nu^*}, \;\; Go = Re^{\frac{1}{4}}\sqrt{\frac{L^*}{R^*}}, \;\; \Lambda = \frac{U_\infty^* \lambda^*}{\nu^*}\sqrt{\frac{\lambda^*}{R^*}},$$

where ν^* denotes the kinematic viscosity, L^* is a plate characteristic length and the freestream velocity is denoted by U_∞^*. The curvature radius of the concave surface is represented by R^* and λ^* denotes the spanwise wavelength.

Assuming that U_∞^* is the potential streamwise velocity at a L^* position from the leading edge and dimensional quantities are identified by an asterisk, non-dimensionalization relations hold for

$$x = \frac{x^*}{L^*}, \;\; y = \frac{y^*}{L^*}, \;\; z = \frac{z^*}{L^*},$$

$$u = \frac{u^*}{U_\infty^*}, \;\; v = \frac{v^*}{U_\infty^*}, \;\; w = \frac{w^*}{U_\infty^*},$$

$$\omega_x = \frac{\omega_x^* L^*}{U_\infty^*}, \;\; \omega_y = \frac{\omega_y^* L^*}{U_\infty^*}, \;\; \omega_z = \frac{\omega_z^* L^*}{U_\infty^*}.$$

The nonlinear functions a, b, c and d shown in Eqs. (1) – (3) are defined by

$$\begin{aligned} a &= \omega_x(v_b + v) - \omega_y(u_b + u), \\ b &= \omega_{zb}u + \omega_z(u_b + u) - \omega_x w, \\ c &= (w_b + w)\omega_y - (v_b + v)\omega_z - \omega_{zb}v, \\ d &= 2u_b u + u^2, \end{aligned}$$

where the derivative of d captures the curvature effects.

The continuity equation is given by

$$\frac{\partial u}{\partial x} + \frac{\partial v}{\partial y} + \frac{\partial w}{\partial z} = 0. \tag{4}$$

From the definition of vorticity and the mass conservation equation, we obtain Poisson equations for each velocity component:

$$\frac{\partial^2 u}{\partial x^2} + \frac{\partial^2 u}{\partial z^2} = -\frac{\partial \omega_y}{\partial z} - \frac{\partial^2 v}{\partial x \partial y}, \tag{5}$$

$$\frac{\partial^2 v}{\partial x^2} + \frac{\partial^2 v}{\partial y^2} + \frac{\partial^2 v}{\partial z^2} = -\frac{\partial \omega_z}{\partial x} + \frac{\partial \omega_x}{\partial z}, \tag{6}$$

$$\frac{\partial^2 w}{\partial x^2} + \frac{\partial^2 w}{\partial z^2} = \frac{\partial \omega_y}{\partial x} - \frac{\partial^2 v}{\partial y \partial z}. \tag{7}$$

Therefore, Eqs. (1) – (3), (4) and (5) – (7) define the system of equations for disturbances. The boundary layer mean flow values are calculated considering the Blasius boundary layer approximation (Schlichting, 1979).

3. NUMERICAL METHOD

The geometry of the numerical domain is sketched in Fig. 2, and the numerical method used to solve the system of the governing equations is based on high order compact finite difference approximations for the discretization of the streamwise and wall normal spatial derivatives (Petri *et al.*, 2015). In the spanwise direction a spectral method based on Fast Fourier transformation was adopted. The time integration was carried out by a classical fourth order Runge-Kutta scheme. A buffer-domain technique was considered to avoid reflection of disturbances at the boundaries.

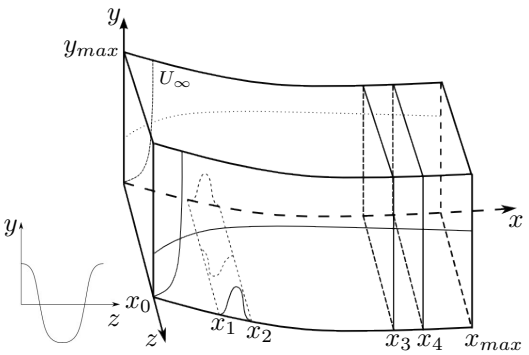

Figure 2. Sketch of the numerical domain

Assuming that there is periodicity in the spanwise direction of the flow we adopted a spectral method. Each total amounts of velocity and vorticity components denoted by $\widetilde{g}$, can be written as a linear combination of the $k+1$ spanwise Fourier modes

$$g(x,y,z,t) = \sum_{k=0}^{K} g_k(x,y,t) e^{-\iota k \beta z}, \tag{8}$$

where ι is the imaginary unit, β denotes the spanwise wavenumber and it is given by $\beta = \dfrac{2\pi}{\lambda}$. Substituting the Fourier transforms given by Eq. (8) in the Eqs. (1) – (3) and (5) – (7), one obtains the governing equations in the Fourier space:

$$\frac{\partial \omega_{x_k}}{\partial t} + \frac{\partial a_k}{\partial y} + \iota k\beta b_k - \iota k\beta d_k \frac{Go^2}{\sqrt{Re}} = \frac{1}{Re}\nabla_k^2 \omega_{x_k}, \tag{9}$$

$$\frac{\partial \omega_{y_k}}{\partial t} - \iota k\beta c_k - \frac{\partial a_k}{\partial x} = \frac{1}{Re}\nabla_k^2 \omega_{y_k}, \tag{10}$$

$$\frac{\partial \omega_{z_k}}{\partial t} + \frac{\partial b_k}{\partial x} - \frac{\partial c_k}{\partial y} - \frac{\partial d_k}{\partial x}\frac{Go^2}{\sqrt{Re}} = \frac{1}{Re}\nabla_k^2 \omega_{z_k}, \tag{11}$$

$$\frac{\partial^2 u_k}{\partial x^2} - k^2\beta^2 u_k = -\iota k\beta \omega_{y_k} - \frac{\partial^2 v_k}{\partial x \partial y}, \tag{12}$$

$$\frac{\partial^2 v_k}{\partial x^2} + \frac{\partial^2 v_k}{\partial y^2} - k^2\beta^2 v_k = -\frac{\partial \omega_{z_k}}{\partial x} - \iota\beta\omega_{x_k}, \tag{13}$$

$$\frac{\partial^2 w_k}{\partial x^2} - k^2\beta^2 w_k = \frac{\partial \omega_{y_k}}{\partial x} + \iota k\beta \frac{\partial v_k}{\partial y}, \tag{14}$$

where $\nabla_k^2 = \left(\frac{\partial^2}{\partial x^2} + \frac{\partial^2}{\partial y^2} - k^2\beta^2\right)$. The nonlinear coupled system of equations given by Eqs. (9) – (14) is solved numerically in the domain shown schematically in Fig. 2. The inflow boundary is represented by $x = x_0$ and the outflow boundary, $x = x_{max}$. Disturbances are introduced into the flow field using spanwise suction and blowing of mass at the wall in a disturbance strip at the wall located in the region between points x_1 and x_2. In order to avoid wave reflections at the outflow boundary we implemented in the region located between x_3 and x_4 a buffer domain technique (Kloker *et al.*, 1993). The calculation of spatial derivatives were done using a high order compact finite difference-schemes (Souza *et al.*, 2005). The v-Poisson equation, defined in Eq. (13), was solved using a multigrid Full Approximation Scheme (FAS) (Stüben and Trottenberg, 1981). For the implementation we adopted a V-cycle working with four levels. The solution will converge, ie, the steady state is reached when the maximum difference between the $k = 1$ spanwise vorticity component is smaller than a given considerably small parameter in two consecutive time steps.

3.1 The boundary conditions

The governing equations defined above are complemented by the follows boundary conditions:

- In $y = 0$, ie., at the wall, we impose a no-slip condition for the streamwise u_k and the spanwise w_k velocity components;
- In the suction and blowing strip region, we specify the wall-normal velocity component at the wall v_k and away from the disturbance generator this velocity component was set to zero;
- The function used for the wall-normal velocity v_1 at the disturbance generator is imposed to have a $\sin^3$ shape;
- In $x = x_0$, the velocity and the vorticity components are zero. In the same way, to $x = x_{max}$, the second derivatives with respect to the streamwise direction of the velocity and vorticity components are set to zero;
- At the upper boundary ($y = y_{max}$) the flow is considered nonrotational. We defined the wall-normal velocity component at $y = y_{max}$ according to the condition: $\left.\frac{\partial v_k}{\partial y}\right|_{x,y_{max},t} = 0$. In addition, at the wall, the condition $\frac{\partial v_k}{\partial y} = 0$ was imposed in the solution of the u_k velocity Poisson equation (Eq. (12));
- The expressions used for calculate the vorticity components at the wall are:

$$\begin{aligned} \frac{\partial^2 \omega_{x_k}}{\partial x^2} - k^2\beta^2\omega_{x_k} &= -\frac{\partial^2 \omega_{y_k}}{\partial x \partial y} - \beta\nabla_k^2 v_k, \\ \omega_{y_k} &= 0, \\ \frac{\partial \omega_{z_k}}{\partial x} &= \iota k\beta\omega_{x_k} - \nabla_k^2 v_k. \end{aligned}$$

4. RESULTS

The simulations have been conducted using physical parameters taken from experiments of Wang *et al.* (1997) and H. P. Wang and Eckert (2005). The pressure side of the experimental turbine blade profile was adapted according to the computational domain considered in the present study. The free stream velocity at $x^* = L = 1.0 \times 10^{-2}\ m$ is $U_\infty^* = 41.806\ ms^{-1}$ and the corresponding Reynolds number is $Re = 2.7704 \times 10^4$, the kinematic viscosity $\nu^* = 1.5 \times 10^{-5}\ m^2 s^{-1}$, the time step $dt = 2 \times 10^{-1} \times dx$, the number of points in the x and y directions are 1305 and 257, respectively. The distance between two consecutive points in the x and y directions are $dx = 1.08 \times 10^{-2}$ and $dy = 5.0 \times 10^{-4}$. The disturbances were introduced in the region $1.53 \leq x \leq 1.99$, with a small amplitude of $A = 1 \times 10^{-10}$. A stretching factor of 1% is adopted in the y-direction. The development of characteristic wavelength vortices with highest amplification rate $\Lambda = 210$ at the positions $x = 5.52$, $x = 8.63$ and $x = 11.53$ corresponding to three different spanwise wavelengths, respectively, $\lambda_1^* = 7.24 \times 10^{-4}\ m$, $\lambda_2^* = 10.631 \times 10^{-4}\ m$ and $\lambda_3^* = 16.414 \times 10^{-4}\ m$ is studied. Figure 3 shows curves of spanwise wavelengths λ^* as a function of wavelength parameter Λ in the streamwise direction. Black squares represent vortices with characteristic wave number $\Lambda = 210$ at three different streamwise positions.

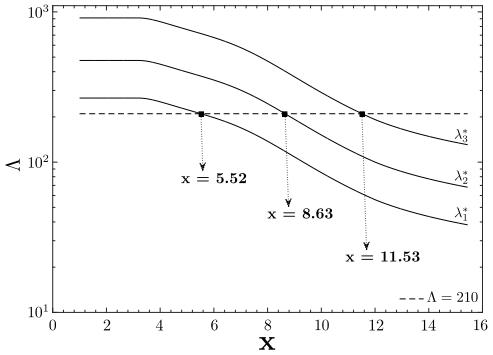

Figure 3. Curves of wavelength parameter Λ to three different spanwise wavelengths λ^*

4.1 Vortex amplification rates and energy streamwise variations of the fundamental mode

A comparison between linear results obtained considering the pressure side of the turbine blade adopted in the numerical simulations of this work and a surface with constant curvature of radius $R = 4.085 \times 10^{-2}\ m$ is presented through

the analysis of the local amplification rate α of the Görtler vortices. Considering variations between the adopted scales (Goulpié *et al.*, 1996), the local amplification rate is given by $\alpha = \alpha_{NS} x$, with

$$\alpha_{NS} = \frac{dE(x)}{dx}\frac{1}{E(x)},$$

where $E(x)$ is a metric to analyze the evolution of disturbances. In the present work, the energy of each Fourier mode is quantified by the integral measures (Benmalek and Saric, 1994)

$$E_k(x) = \int_0^\infty |u_k|^2 \, dy, \; 0 \leq k \leq K-1.$$

For nonlinear simulations, we define $K = 11$. For linear simulations, just the fundamental mode $(k = 1)$ is considered.

The evolution of the characteristic wavelength vortices with highest amplification rate $\Lambda = 210$ at the positions $x = 5.52$, $x = 8.63$ and $x = 11.53$ corresponding to three different spanwise wavelengths, respectively, $\lambda_1^* = 7.24 \times 10^{-4}\ m$, $\lambda_2^* = 10.631 \times 10^{-4}\ m$ and $\lambda_3^* = 16.414 \times 10^{-4}\ m$ is illustrated in the Fig. 4. In this figure it is possible to see a growth of the disturbances in a wall with constant curvature (Fig. 4b) to all wavelength cases. At inflow where the curvature of the wall has a constant radius for both wall cases studied, the energy of the vortices grow linearly. From a given position of the domain where the radius of the turbine blade becomes variable, this growth becomes small when compared to the case where the curvature is constant.

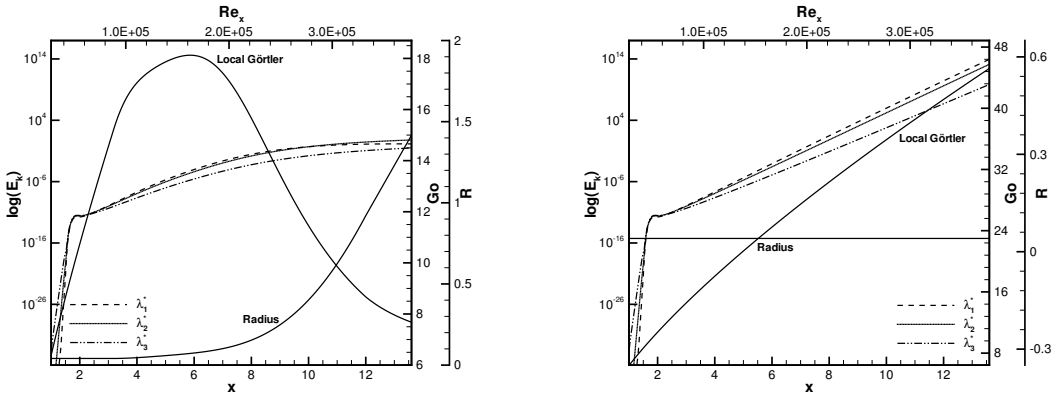

(a) Variable curvature (b) Constant curvature

Figure 4. Energy distribution to fundamental mode in the streamwise direction

The local amplification rate for these vortices is plotted against x in the Fig. 5. In accordance with what has been discussed previously, Fig. 5 shows an amplification of the vortices at inflow where the radius of the curvature is constant for both cases studied. Observe that a sharp decrease in vortex amplification rates occurs in the variable curvature case (Fig. 5a), and for the case where the curvature of the wall is constant the vortices remains amplified. The local Görtler number and the the radius distribution of the curvatures adopted were been displayed in Figs. 4 and 5. For the variable curvature, the local Görtler number reaches a maximum value corresponding to 18.13 at $x = 5.88$ and decreases with the increase in the radius of the blade.

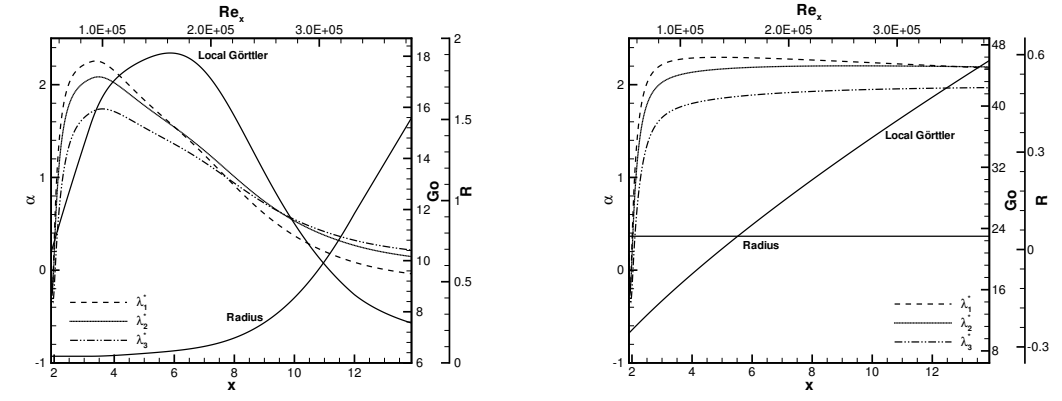

(a) Variable curvature (b) Constant curvature

Figure 5. Dimensionless spatial amplification rates

4.2 The non-linear evolution of Görtler vortices over the turbine blade pressure side

For the nonlinear study of the evolution of Görtler vortices, $k + 1 = 11$ Fourier modes and 32 points in the physical space has been adopted. Other physical parameters were defined as explained at the beginning of this section.

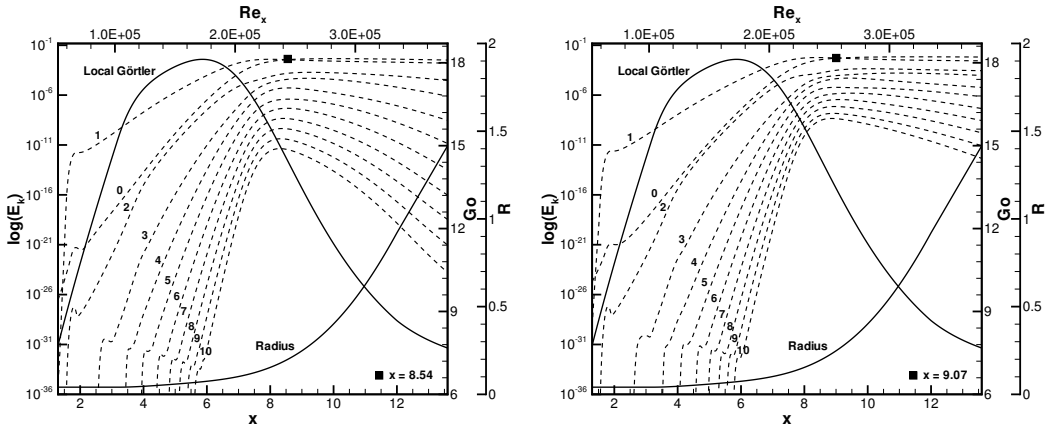

(a) $\lambda_1^* = 7.24 \times 10^{-4}\ m$

(b) $\lambda_2^* = 10.631 \times 10^{-4}\ m$

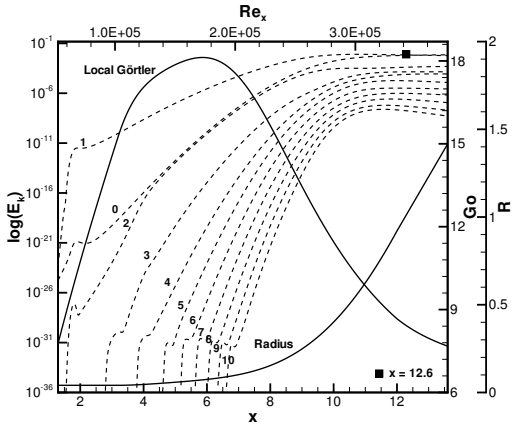

(c) $\lambda_3^* = 16.414 \times 10^{-4}\ m$

Figure 6. Streamwise evolution of each Fourier mode for vortices with three different spanwise wavelengths λ^*. Black squares identify locations where energies of the mean flow distortion (mode $k = 0$) and the fundamental mode (mode $k = 1$) become equal

In Fig. 6 the energy for all Fourier modes $k = 0, \ldots, 10$ is presented for the development of $\Lambda = 210$ vortices, considering three different spanwise wavelengths $\lambda_1^* = 7.24 \times 10^{-4}\ m$, $\lambda_2^* = 10.631 \times 10^{-4}\ m$ and $\lambda_3^* = 16.414 \times 10^{-4}\ m$. For all cases, the fundamental mode ($k = 1$) shows the highest energy level in the linear region. The regions defined by $2 \leq x \leq 8.29$ (to see Fig. 6a), $2 \leq x \leq 8.5$ (to see Fig. 6b) and $x \geq 2$ (to see Fig. 6c) are characterized by exponential growth of the Görtler vortices. Furthermore downstream nonlinear effects become more significant, and saturation occurs in position $x = 8.54$ (black square in Fig. 6a), $x = 9.07$ (black square in Fig. 6b) and $x = 12.6$ (black square in Fig. 6c). In the saturation region, the difference between the amplitude of consecutive modes are almost constant, and the amplitudes of the last modes are very small. By means of Fig. 6, and based on the saturation criterion proposed in this work, it is noted that the saturation is postponed as a function of an increase in the spanwise wavelength.

Table 1. Values of λ^*, x and E_k.

$\lambda^* \times 10^{-4}\ m$	x	E_k
7.24	8.54	3.6×10^{-3}
10.631	9.07	5.1×10^{-3}
16.414	12.6	6.6×10^{-3}

In Tab. 1, x stands for the streamwise location where the energies of the fundamental ($k = 1$) and the mean flow distortion ($k = 0$) modes are equal and E_k stands for the corresponding modal energy.

Considering three different spanwise wavelengths, Figs. 7, 8 and 9 display the the spatial evolution of the hydrodynamic boundary layer. These figures show the isovelocity distribution for the component u from 0.1 to 0.9 in crosscut planes $z \times y$. The streamwise crosscut positions are been defined at $x = 7$, $x = 10$ and $x = 13$.

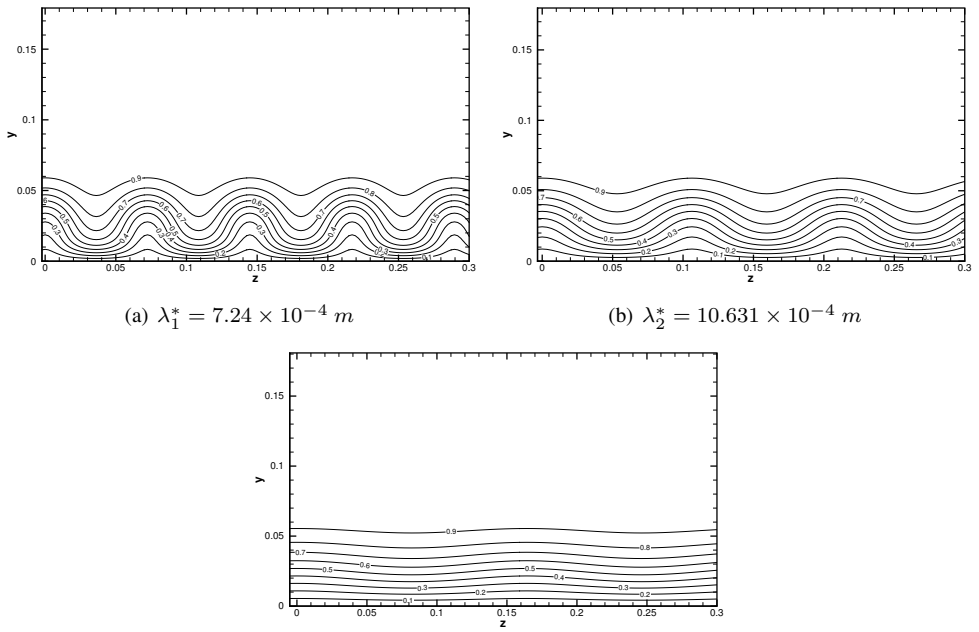

(a) $\lambda_1^* = 7.24 \times 10^{-4}\ m$ (b) $\lambda_2^* = 10.631 \times 10^{-4}\ m$

(c) $\lambda_3^* = 16.414 \times 10^{-4}\ m$

Figure 7. Distributions of $u-$velocity component in the $(z, y)-$plane for vortices with three different λ^* at streamwise position $x = 7$

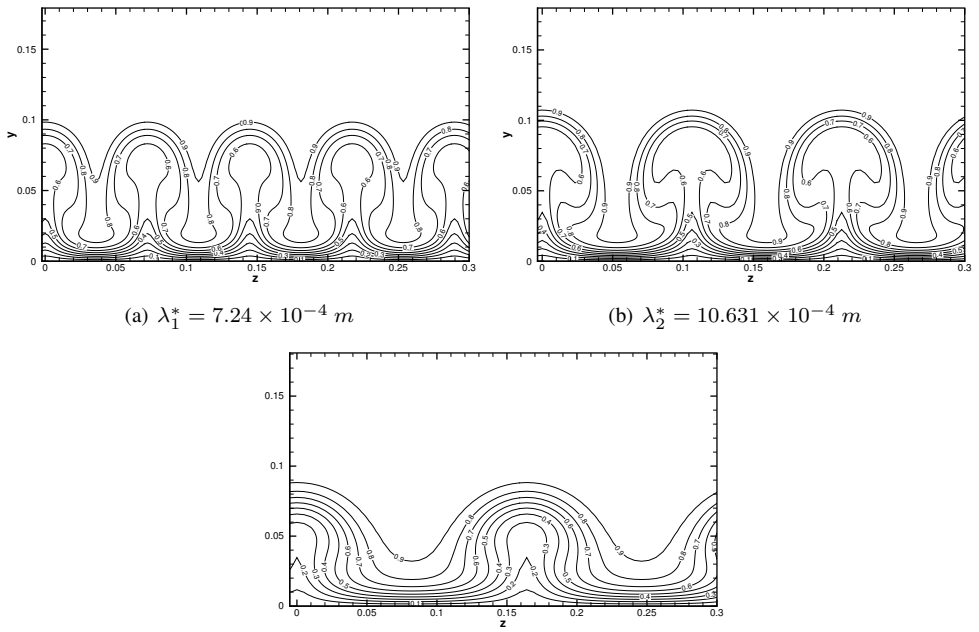

(a) $\lambda_1^* = 7.24 \times 10^{-4}\ m$ (b) $\lambda_2^* = 10.631 \times 10^{-4}\ m$

(c) $\lambda_3^* = 16.414 \times 10^{-4}\ m$

Figure 8. Distributions of $u-$velocity component in the $(z, y)-$plane for vortices with three different λ^* at streamwise position $x = 10$

The mushroom structure typical for Görtler flow can be clearly observed on Figs. 8a and b, Figs. 9a, b and c. The other cases shown in Figs. 7, 8 and 9 the mushroom shape can not be noted because at these crosscut position the vortices are not saturated yet, which means that the non-linear effects do not yet become predominant. In a flow with Görtler

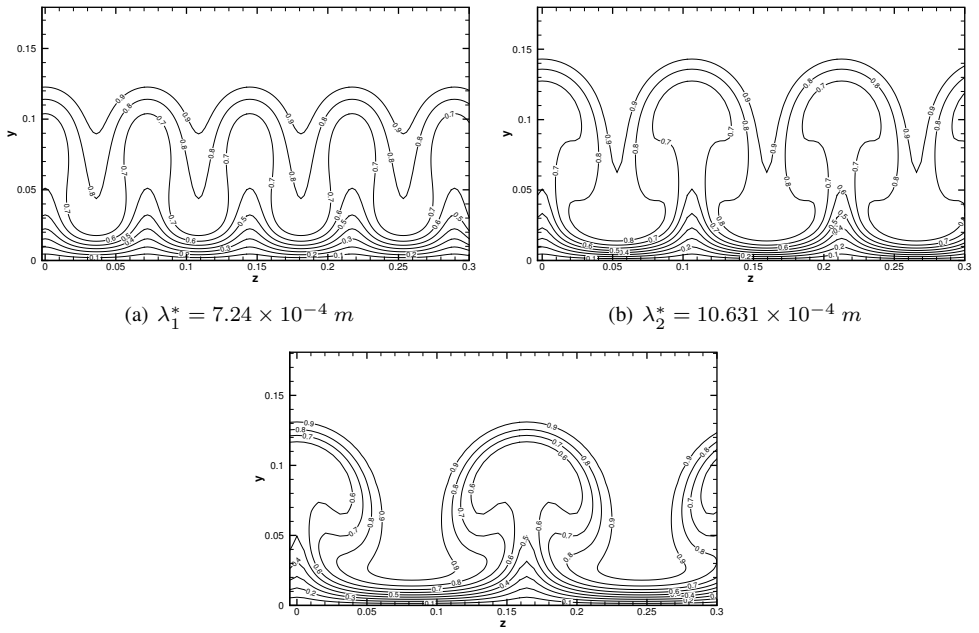

(a) $\lambda_1^* = 7.24 \times 10^{-4}\ m$ (b) $\lambda_2^* = 10.631 \times 10^{-4}\ m$

(c) $\lambda_3^* = 16.414 \times 10^{-4}\ m$

Figure 9. Distributions of $u-$velocity component in the $(z, y)-$plane for vortices with three different λ^* at streamwise position $x = 13$

vortices two regions can be seen, the upwash and downwash regions. In the downwash region the vortices pump high velocity flow to a region close to the wall, smashing the boundary layer. In the upwash region the opposite occurs. In the nonlinear region, it is possible to see that the downwash region is wider than the upwash region.

5. CONCLUSIONS

In the present study the linear and nonlinear aspects of the Görtler instability evolution in turbine blades were investigated by means of high-order numerical simulations. A comparison of the local amplification rate α of the Görtler vortices obtained considering the pressure side of the turbine blade and a fully concave wall surface with radius equal $4.085 \times 10^{-2}\ m$ showed that there is a greater amplification of the vortices for the case where the wall has a constant curvature independent of the spanwise wavelength. For the analysis of the nonlinear effects in the evolution of the Görtler vortices, it was observed the size of the vortical structures is an important parameter on transition process, where the most dangerous case analyzed was $\lambda_1^* = 7.24 \times 10^{-4}\ m$.

6. ACKNOWLEDGEMENTS

The authors acknowledge Brazilian Federal Agency for Support and Evaluation of Graduate Education (CAPES).

7. REFERENCES

Benmalek, A. and Saric, W.S., 1994. "Effects of Curvature Variation on the Nonlinear Evolution of Goertler Vortices". *Physics of Fluids*, Vol. 6, pp. 3353–3367.

Goulpié, P., Klingmann, B. and Bottaro, A., 1996. "Görtler vortices in boundary layers with streamwise pressure gradient". *Physics of Fluids*, Vol. 8, pp. 451–459.

H. P. Wang, S. J. Olson, R.J.G. and Eckert, E.R.G., 2005. "Development of taylor-görtler vortices over the pressure surface of a turbine". *Transactions of the ASME*, Vol. 127, pp. 541–543.

Kloker, M., Konzelmann, U. and Fasel, H., 1993. "Outflow boundary conditions for spatial Navier-Stokes simulations in transition boundary layers". *AIAA Journal*, Vol. 31, pp. 620–628.

Petri, L., Sartori, P., Rogenski, J.K. and Souza, L.F., 2015. "Verification and validation of a Direct Numerical Simulation code". *Computer methods in applied mechanics and engineering*, Vol. 291, pp. 266–279.

Schlichting, H., 1979. *Boundary-Layer Theory*. McGraw-Hill, IncH.

Souza, L.F., Mendonça, M.T., de Medeiros, M.A.F. and Kloker, M., 2004. "Seeding of Görtler vortices through a suction and blowing strip". *Journal of the Brazilian Society of Mechanical Sciences*, Vol. XXVI, pp. 269–279.

Souza, L.F., Mendonça, M.T. and Medeiros, M.A.F., 2005. "The advantages of using high-order finite differences schemes

in laminar-turbulent transition studies". *International Journal for Numerical Methods in Fluids*, Vol. 48, pp. 565–592.

Stüben, K. and Trottenberg, U., 1981. *Nonlinear multigrid methods, the full approximation scheme*, Köln-Porz, chapter 5, pp. 58–71. Lecture Notes in Mathematics.

Wang, H.P., Olson, S.J., Goldstein, R.J. and Eckert, E.R.G., 1997. "Flow visualization in linear turbine cascade of high performance turbine blades". *ASME J. Turbomach.*, Vol. 19, p. 0108.

8. RESPONSIBILITY NOTICE

The authors L. F. Marques, J. K. Rogenski and L. F. de Souza are the only responsible for the printed material included in this paper.